RSC Advances

PAPER

Cite this: *RSC Adv.*, 2020, **10**, 12883

Synthesis of an ordered nanoporous Cu/Ni/Au film for sensitive non-enzymatic glucose sensing†

Gang Liu, Jianwei Zhao,* Lirong Qin, Song Liu, Qitao Zhang and Junxian Li

Received 8th February 2020
Accepted 24th March 2020

DOI: 10.1039/d0ra01224f

rsc.li/rsc-advances

Ordered nanoporous Cu/Ni/Au film was prepared by electrochemical deposition and magnetron sputtering using an anodic aluminium oxide template. The fabricated porous film has a uniform hexagonal pore size structure, a long-range ordered arrangement, and a pore diameter of approximately 40 nm. Following the dissolution of the template, the independent Cu/Ni/Au film is devolved to an ITO substrate as an effective non-enzyme glucose detection sensor. The sensor has good electrocatalytic performance with two specific linear ranges of 0.5 μM to 3.0 mM and 3.0–7.0 mM and high sensitivities of 4135 and 2972 μA mM^{-1} cm^{-2}, respectively. The lower detection limit was 0.1 μM with a signal-to-noise ratio of 3. Additionally, the sensor features excellent selectivity and stability. These satisfactory results indicate that Cu/Ni/Au film is a promising platform for the development of non-enzymatic glucose sensors.

Introduction

Glucose, the primary energy source and metabolic intermediate for living organisms, is called blood sugar in the human body and is a leading cause of diabetes when found in high concentrations. Diabetes mellitus is one of the most common and frequently occurring diseases in the world and seriously threatens human health.[1,2] Heart disease, renal failure, and blindness are some of the many complications of diabetes which can be effectively prevented and controlled by the timely monitoring of blood sugar levels. Therefore, the development of a fast, accurate, convenient, reproducible, and stable glucose detection method is of great significance in pathology, physiology, medicine, and bionics.[3,4] Researchers have developed a variety of optical,[5] acoustic,[6] transdermal,[7] and electrochemical methods to accurately detect glucose. Electrochemical methods are considered the most suitable because of their easy monitoring, high sensitivity, and simplicity.[8,9] Most of the currently available electrochemical glucose biosensors are based on enzyme analysis because of their sensitivity and fast detection speed. However, the enzyme sensor is unstable because temperature, pH, humidity, detergents, and toxic chemicals[10,11] affect the activity of glucose oxidase. Thus, the development of non-enzymatic glucose sensors with a low detection limit and wide response range is of great interest.[12–15]

The nanostructure-based non-enzymatic detection of glucose employs the superior catalytic properties of nanomaterials.[16–19] Copper and nickel nanostructures attract increasing attention for their low cost and remarkable catalytic performance through the redox coupling of divalent/trivalent ions in alkaline solution.[20–23] Most Cu- or Ni-based non-enzymatic glucose sensors are prepared by modifying substrates with nanoparticles, scattered structures, or metal/carbon hybrids.[24] Ordered nanoporous film, which has a large active surface area and an ordered arrangement of nanoscale pores, has received considerable attention in recent years for its particular properties and promising utilisation in optoelectronic devices, photonic crystals, and catalysis.[25–28] However, reports on the application of nanoporous film for the detection of glucose are still scarce. In this study, ordered nanoporous Cu/Ni/Au film was prepared by electrochemical deposition and magnetron sputtering using an anodic aluminium oxide template. After dissolving the template, the nanoporous Cu/Ni/Au film was transferred onto ITO glass to be used as an effective non-enzymatic glucose sensor. It exhibits good performance with high sensitivity, a wide linear range, and a low detection limit because of its porous structure and composite material.

Experimental section

Chemicals and reagents

Glucose, ascorbic acid, uric acid, and dopamine were obtained from Sigma-Aldrich Chemical Company. Acetone, ethanol, phosphoric acid, oxalic acid, and other analytical grade chemicals were purchased from Chongqing Chuandong Chemical Company. Deionised water was used throughout the experiments. The electrochemical measurements were carried out on a CHI 660E three-electrode system electrochemical analyser with a modified working electrode. An Ag/AgCl electrode served as the reference, and a Pt wire electrode as the counter. All experiments were performed at ambient temperature (20 ± 1

School of Physical Science and Technology, Southwest University, Chongqing 400715, P. R. China. E-mail: zhaojw@swu.edu.cn

† Electronic supplementary information (ESI) available. See DOI: 10.1039/d0ra01224f

°C). The as-synthesised products were characterised by scanning electron microscopy (SEM, JSM-7100F), X-ray diffraction (XRD, TD-3500), and transmission electron microscopy (TEM, FEI Tecnai G20) with selected area electron diffraction (SAED) patterns.

Synthesis of nanoporous Cu/Ni/Au film

The AAO templates were homemade by the anodisation process described in previous reports.[29,30] In this work, the anodisation was carried out at 45 V for 6 h in 0.3 M (mol L^{-1}) oxalic acid electrolyte. The distance between the two adjacent channels in the templates was approximately 115 nm, and the diameter of the channels was approximately 60 nm. The preparation of the nanoporous Cu/Ni/Au film is illustrated in Scheme 1. An Au layer with a thickness of approximately 50 nm was sputtered onto the top side of the template by an advanced sputter coater (ETD-2000) equipped with a high-purity Au (99.999%) target. The deposition process was performed under a rarefied air with a pressure of 10 Pa. The deposition time was about 15 min with a direct-current of 5 mA. The template sputtered with Au film served as the working electrode in the subsequent electrochemical deposition. Ni was deposited by the two-electrode method using carbon block as the anode. The composition of the deposition solution was 80 g L^{-1} $NiSO_4 \cdot 6H_2O$, 20 g L^{-1} H_3BO_3, and 1.5 g L^{-1} $C_6H_8O_7 \cdot H_2O$ dissolved in 100 mL of deionised water. The deposition process underwent constant current deposition of 1.0 mA for 5 minutes. After deposition, the template was completely dissolved in deionised water for 1 hour and dried in a Petri dish at room temperature. Afterwards, a surface layer of Cu with a thickness of approximately 15 nm was deposited on the template by a magnetron sputtering system (VTC-16-SM) equipped with a high-purity Cu (99.999%) metal target. The pressure was evacuated to about 5 Pa in N_2 atmosphere. The deposition process was performed under a power of 60 W. The deposition time was about 10 min. All above experiments were carried out at ambient temperature (20 ± 1 °C). The nanoporous Cu/Ni/Au film was obtained at the surface of the AAO template. The above process controlled the thickness of the film; if the gold, nickel and copper films are too thick, the final product loses its porous structure.

Electrode fabrication

The ordered nanoporous Cu/Ni/Au film was floated on the surface of the 2 mol L^{-1} NaOH aqueous solution for several minutes to separate the film from the AAO. A soft, free, continuous metal film was obtained from the dissolution of the AAO template. The metal film was subsequently transferred to the ITO glass using suspension transfer technology.[31] When the transferred film was completely dry, a strong binding force formed between the film and the ITO glass, which guarantees the feasibility of practical applications of the film. Next, epoxy resin was encapsulated on the ITO glass to prevent the shedding of porous film and to avoid contact between the ITO and the test solution. As a result, the effective area of nanoporous Cu/Ni/Au film was approximately 6.0 mm^2. In comparison, nanoporous Cu/Au and Ni/Au films were prepared and transferred to the ITO glass and then encapsulated by epoxy resin to maintain a similar effective area.

Results and discussion

Characterisation of the porous film

Fig. 1a shows the top view SEM image of the AAO template sputtered with the Au layer. The template is arranged in an ordered hexagonal close-packed pores array which maintains the AAO template's geometrical ordering. The magnified image in Fig. 1b shows that the porous Au film is mountain-shaped with surface peaks and valleys. The distance to the adjacent pores is about 115 nm and matches that of the template. Each pore is enclosed by six mounds and reveals an average diameter of approximately 50 nm. After depositing the Ni layer through secondary electrodeposition, the product—Ni/Au nanoporous film—maintains the same ordered morphology as the AAO template as shown in Fig. 1c. The high-magnification SEM image (Fig. 1d) clearly shows that the Ni/Au film is thicker than the former product. The thickness of the Ni layer is estimated to about 40 nm. The Ni/Au film now appears to be rugged with numerous pits spreading across its surface.

Fig. 2a and b show an overview SEM image of the product after deposition of the Cu surface layer by magnetron sputtering. The final product is also arranged in an ordered hexagonal close-packed pores array and maintains the AAO template's geometrical ordering. The porous film, magnified in Fig. 2c,

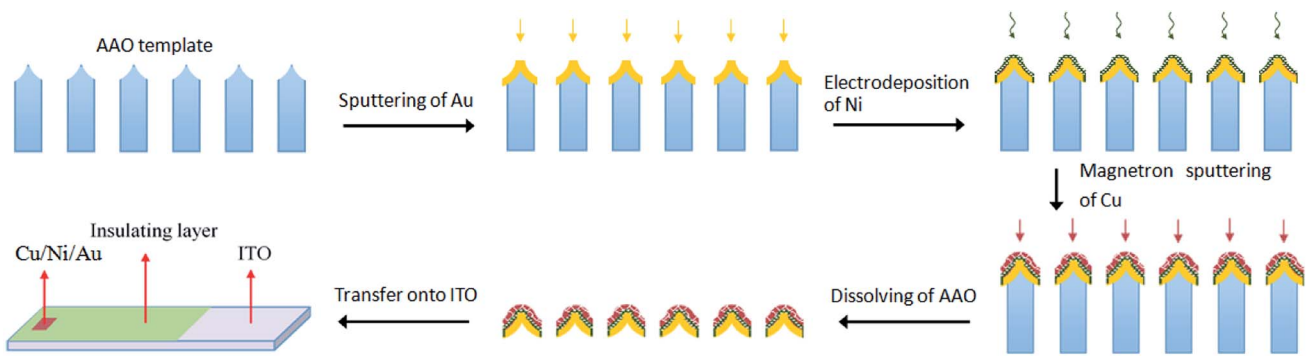

Scheme 1 Illustration of the fabrication of the ordered nanoporous Cu/Ni/Au array film.

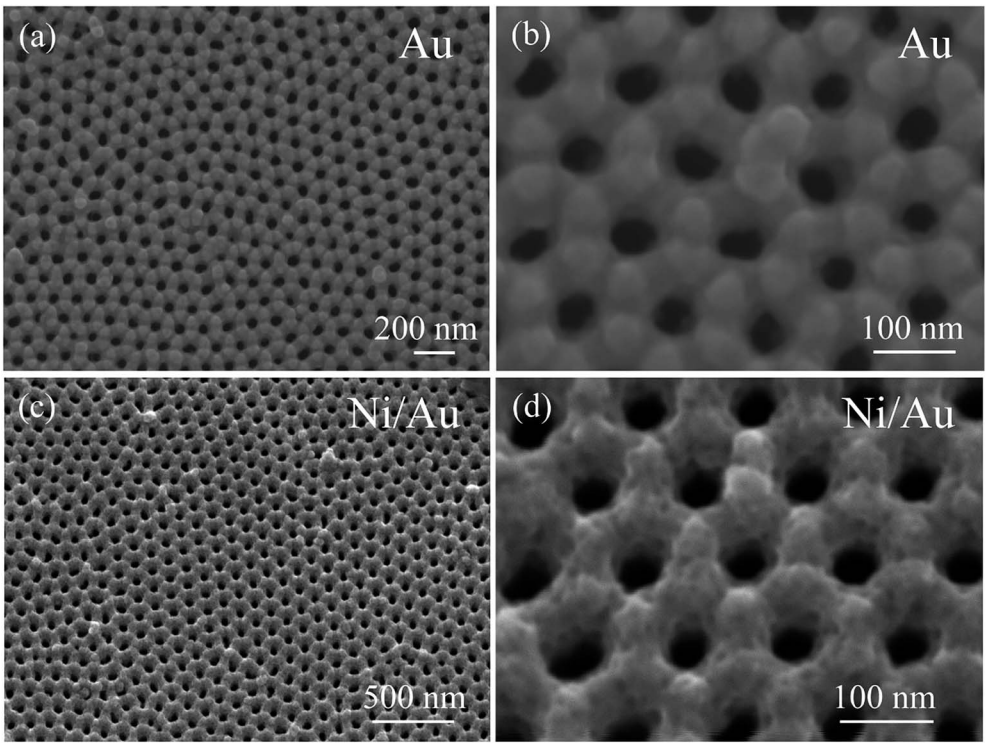

Fig. 1 (a and b) SEM images in top view of the AAO template sputtered with Au layer, (c and d) the SEM images of the nanoporous Ni/Au film.

indicates that the adjacent pores—at a distance of approximately 115 nm—match those of the template, and that each pore has a diameter of approximately 40 nm. The final porous film consists of a layer of fine Cu grains, which cause rugged

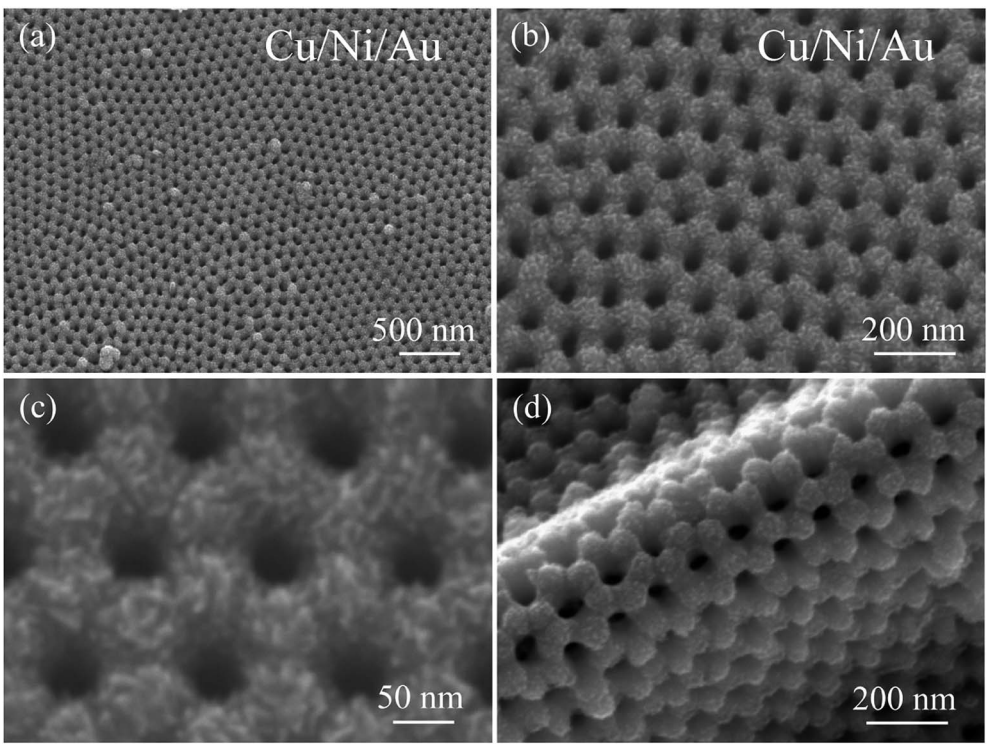

Fig. 2 (a) Low-magnification SEM image of the nanoporous Cu/Ni/Au film, (b and c) the high-magnification SEM image, (d) SEM image showing the bent porous Cu/Ni/Au film.

surface topography and greatly increase the surface area. Fig. 2d shows that the final nanoporous Cu/Ni/Au film separated from the template can be bent 180° without causing breakage, indicating that our nanoporous film is potentially applicable as a flexible sensor electrode. Additionally, the vertical height of the rolling film is approximately 135 nm. In contrast, the nanoporous Cu/Au film was prepared by the two-step deposition method. SEM images of the Cu/Au film are provided in Fig. S1 (ESI†). It can be found that this sample shows a similar morphology to that of the porous Cu/Ni/Au film.

Fig. 3a depicts a typical TEM image of the nanoporous Cu/Ni/Au film. The final product shows the uniform pore size and long-distance ordered arrangement of a hexagonal structure. The high-magnification TEM image in Fig. 3b faintly shows that the nanoporous Cu/Ni/Au film is composed of polycrystalline grains with a length of 10–20 nm. The corresponding SAED (selected area electron diffraction) pattern (Fig. 3c) confirms the polycrystalline appearance of the porous film. EDS attached to TEM was used to investigate the chemical composition of the final product. The very strong Pt and Cu peaks and the weak Ni peaks, shown in the spectrum in Fig. 3d, indicate the formation of the Cu/Ni/Au film.

Porous film properties

After immobilisation onto the ITO glass, the ordered porous Cu/Ni/Au film can be directly used as a non-enzymatic sensor electrode for the detection of glucose. The cyclic voltammogram (CV) curves of the Cu/Ni/Au film electrode were experimentally measured in a 0.2 M NaOH solution in the presence and absence of 1 mM glucose at a scan rate of 100 mV s^{-1} to investigate electrocatalytic activity. An increased oxidation peak at approximately 0.6 V is observed (Fig. 4a) when glucose (curve b) is added to the system; the increase indicates the strong electrocatalytic activity of the porous Cu/Ni/Au film electrode towards the oxidation of glucose. As a contrast, the CV curves of the porous Cu/Au film electrode in the presence and absence of glucose were shown in Fig. S2a (ESI†). As expected, an increase of oxidation peak was also observed at tht potential of about 0.6 V. So the principal reaction mechanism for these two electrodes consists of the electro-oxidation of glucose with Cu(III) similar to the previous reports.[31,32] The following scheme explains the possible catalytic mechanism:

$$Cu + 2OH^- \rightarrow Cu(OH)_2 + 2e^- \quad (1)$$

$$Cu(OH)_2 + OH^- \rightarrow CuO(OH) + H_2O + e^- \quad (2)$$

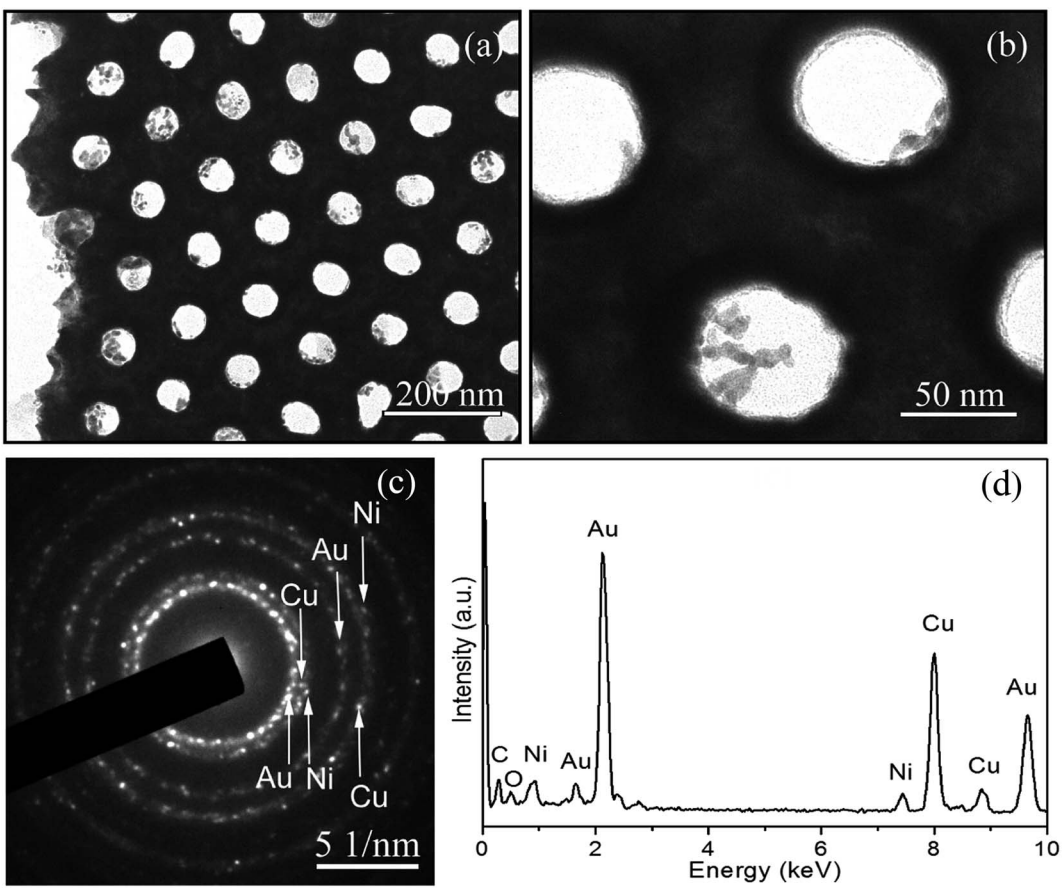

Fig. 3 (a) TEM image of the nanoporous Cu/Ni/Au film, (b) high-magnification TEM image, (c) corresponding SAED pattern, (d) EDS data of the nanoporous Cu/Ni/Au film.

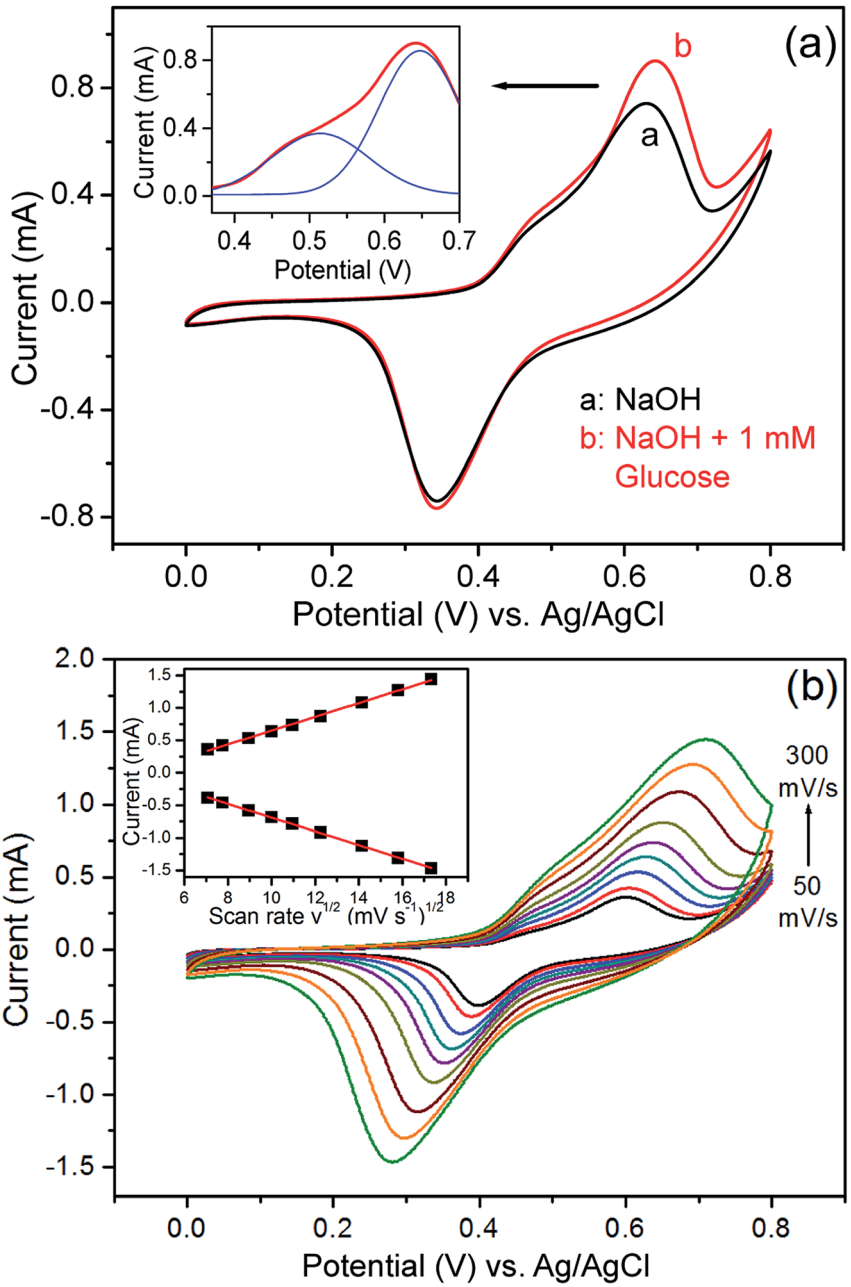

Fig. 4 (a) CV curves of the nanoporous Cu/Ni/Au film in the absence (curve a) and presence (curve b) of glucose in 0.2 M NaOH solution. Inset: multi-peaks Gaussian fitting of the oxidation peak. (b) Typical CVs of the modified electrode in 0.2 M NaOH solution containing 0.5 mM glucose at different scan rates (from 50 to 300 mV s^{-1}). Inset: plots of peak currents *vs.* $v^{1/2}$.

$$CuO(OH) + glucose \rightarrow Cu(OH)_2 + glucolactone \quad (3)$$

It is noteworthy that a weak enhancement of oxidation peak at about 0.5 V can be identified for the CV curves of the Cu/Ni/Au film electrode (Fig. 4a). This variation can also be observed in the CV curves of the porous Ni/Au film electrode as shown in Fig. S2b (ESI†). Accordingly, we believe that the sensor reaction mechanism involves the electro-oxidation of glucose on Ni exposed between the interspaces of Cu grains on the surface. The activation proceeds as follows:[33,34]

$$Ni + 2OH^- \rightarrow Ni(OH)_2 + 2e^- \quad (4)$$

$$Ni(OH)_2 + OH^- \rightarrow NiO(OH) + H_2O + e^- \quad (5)$$

$$NiO(OH) + glucose \rightarrow Ni(OH)_2 + glucolactone \quad (6)$$

The effect of the potential scan rate was studied using a 0.2 M NaOH solution containing 0.5 mM of glucose (Fig. 4b). The results show that both the oxidation and reduction peak currents increase linearly with respect to the square root of the scanning rate in the 50–300 mV s^{-1} range and indicate that

a diffusion-controlled process occurred on the modified electrode.[35]

Amperometry was also used to study the properties of the porous Cu/Ni/Au film electrode. Fig. 5a shows the amperometric current responses for the film electrode with each addition of 0.5 mM of glucose stirred into an NaOH solution at a constant potential of 0.66 V. The film electrode current rapidly increased and stabilised less than 5 s after the glucose was injected and demonstrated the sensitive response to changes in glucose concentration. In contrast, the double-layered nanoporous Cu/Au film and the nanoporous Ni/Au film show much lower glucose detection activity, revealing that there should be a synergetic effect from combining Cu with Ni in the oxidation reaction between the Cu/Ni/Au film and glucose. Fig. 5b shows that a small amount of added glucose causes a notable change in the current. The detection limit is 0.1 μM at a signal-to-noise ratio of 3. The inset in Fig. 5 shows the linearity between the peak current and concentration of glucose after a series of tests. The linear fit formulas are:

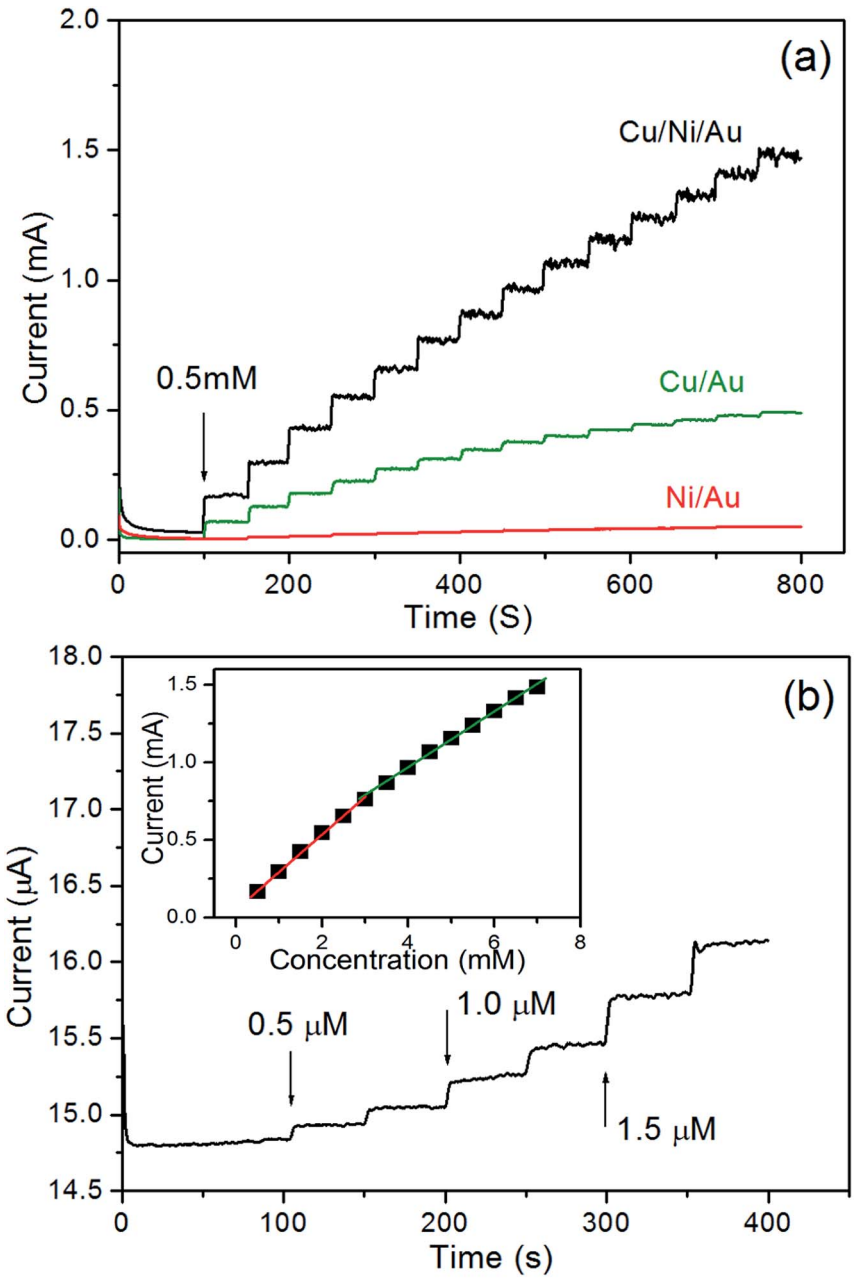

Fig. 5 (a) Typical steady-state current–time response for the nanoporous Cu/Ni/Au film, the nanoporous Cu/Au film, and the nanoporous Ni/Au film, to successive additions of 0.5 mM glucose in 0.2 M NaOH solution at an applied potential of 0.66 V *vs.* Ag/AgCl, (b) the current–time responses for the nanoporous Cu/Ni/Au film to successive additions of the small amount of glucose, inset: the linear relationship of the nanoporous Cu/Ni/Au film between the catalytic current and the glucose concentration.

$$I\,(\mu A) = 248.1 C_{glucose}\,(\mu M) + 40.2 \quad (7)$$

$$I\,(\mu A) = 178.3 C_{glucose}\,(\mu M) + 254.0 \quad (8)$$

The sensitivity is 4135 μA mM^{-1} cm^{-2} (eqn (7)) in the 0.5 μM to 3.0 mM ($R^2 = 0.9981$) range and 2972 μA mM^{-1} cm^{-2} (eqn (8)) in the 3.0–7.0 mM ($R^2 = 0.9988$) range. Table 1 shows the performance comparison of the previously reported glucose sensors prepared using Cu- and Ni-based nanomaterials.[36–42] The porous Cu/Ni/Au film electrode clearly reports a high sensitivity, a low detection limit, and a wide linear range.

The perfect reported performances of the electrode should be related to the distinctive structure of nanoporous Cu/Ni/Au film. Firstly, the specific surface of the porous film fabricated by the AAO template exhibited an ordered, rugged, and porous micro-morphology which produced a higher specific surface area.[28] The larger contact area between the sensing materials and the sensed species provides an excellent sensing performance. Secondly, Cu and Ni are ideal sensor materials and show both reversible reduction and oxidation of trivalent ions.[42] The synergetic effect of combining Cu and Ni might further increase the catalytic performance of the multilayer nanowires and promote the oxidation of glucose. Thirdly, as a type of metal multilayer film, the excellent conductivities of Cu, Ni, and Au could promote the charge transfer from the active reaction sites to the ITO electrode during the electrocatalytic reaction.

To study the reproducibility of the nanoporous Cu/Ni/Au film electrode, three samples were prepared under the same experimental conditions. Electrochemical measurements were carried out and the results indicated that the relative standard deviation (RSD) of the current response to glucose was no more than 4.5% for these samples. The effect of common interfering species coexisting on the porous Cu/Ni/Au film was also examined under the same experimental conditions. As shown in Fig. 6, the addition of 10 μM glucose to the 0.2 M NaOH solution significantly increased response sensitivity. Compared to glucose, the addition of 10 μM of L-cysteine, uric acid (UA), dopamine, and ascorbic acid (AA) did not produce an obvious amperometric response. When not in use, the porous Cu/Ni/Au film electrode was stored in dry conditions. After three weeks of storage, the current response of the sensor showed long-term stability by maintaining approximately 90% of the original response.

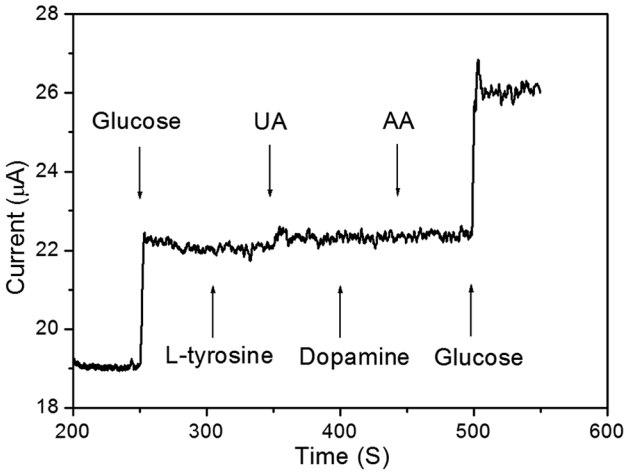

Fig. 6 Amperometric curve of addition of 10 μM glucose, L-cysteine, uric acid, dopamine, and ascorbic acid in 10 mL 0.2 M NaOH solution.

Conclusion

In this study, we described an ordered nanoporous Cu/Ni/Au film fabricated by a three-step deposition method with the assistance of an AAO template. Following the dissolution of the template, the film was transferred onto ITO glass and used as an effective non-enzymatic glucose sensor. The fabricated sensor has good electrocatalytic performance with very high sensitivity, a wide linear range, and a low detection limit. We believe that nanoporous Cu/Ni/Au film provides a promising platform for the development of non-enzymatic glucose sensors.

Conflicts of interest

There are no conflicts to declare.

Table 1 Comparison of some nonenzymatic glucose sensors based on Cu or Ni nanomaterials

Type of electrode	Sensitivity (μA mM^{-1} cm^{-2})	Linear range (μM)	Detection limit (μM)	Reference
Ni nanowires array	1043	0.5–7000	0.1	36
Flower-like CuO hierarchical film	3252	5–2000	0.6	37
CuNi-NPs-3D-KSCs	19.16	7–23 670	2.3	38
CuO_x/Cu nanowire array	1210	10–7000	10	39
Au/Ni multilayer nanowire array	3372	0.25–2000	0.1	30
	1906	2000–5500		
CuNi/MWCNTs	2437	2000–8000	0.025	40
Ni–Cu/TiO_2/GC	719.9	100–6000	30	41
Ni/Cu bowl-like array film	3924	0.5–2500	0.05	42
Cu/Ni/Au nanoporous film	4135	0.5–3000	0.1	This work
	2972	3000–7000		

Acknowledgements

This work was supported by the Natural Science Foundation Project of CQ CSTC (Grant No. cstc2019jcyj-msxmX0311) and the Fundamental Research Funds for the Central Universities (grant XDJK2018B033 and XDJK2020B055).

References

1 J. Wang, *Chem. Rev.*, 2008, **108**, 814–825.
2 E. H. Yoo and S. Y. Lee, *Sensors*, 2010, **10**, 4558–4576.
3 S. B. Bankar, M. V. Bule and R. S. Singhal, *Biotechnol. Adv.*, 2009, **27**, 489–501.
4 K. Tian, M. Prestgard and A. Tiwari, *Mater. Sci. Eng. C*, 2014, **41**, 100–118.
5 J. C. Pickup, F. Hussain, N. D. Evans, O. J. Rolinski and D. J. S. Birch, *Biosens. Bioelectron.*, 2005, **20**, 2555–2565.
6 R. Weiss, Y. Yegorchikov, A. Shusterman and I. Raz, *Diabetes Technol. Therapeut.*, 2007, **9**, 68–74.
7 M. J. Tierney, J. A. Tamada, R. O. Potts, L. Jovanovic and S. Garg, *Biosens. Bioelectron.*, 2001, **16**, 621–629.
8 B. Z. Zheng, G. Y. Liu, A. W. Yao, Y. L. Xiao, J. Du, Y. Guo, D. Xiao, Q. Hu and M. M. F. Choi, *Sens. Actuators, B*, 2014, **195**, 431–438.
9 A. A. Saei, J. E. N. Dolatabadi, P. Najafi-Marandi, A. Abhari and M. de la Guardia, *TrAC, Trends Anal. Chem.*, 2013, **42**, 216–227.
10 E. H. Yoo and S. Y. Lee, *Sensors*, 2010, **10**, 4558–4576.
11 E. Katakis and Z. Domingue, *Trends Anal. Chem.*, 1995, **14**, 310–319.
12 K. Tian, M. Prestgard and A. Tiwari, A review of recent advances in nonenzymatic glucose sensors, *Mater. Sci. Eng. C*, 2014, **41**, 100–118.
13 H. Wei and E. K. Wang, *Chem. Soc. Rev.*, 2013, **42**, 6060–6093.
14 G. Wang, X. He, L. Wang, A. Gu, Y. Huang, B. Fang, B. Geng and X. Zhang, *Microchim. Acta*, 2013, **180**, 161–186.
15 X. H. Kang, Z. B. Mai, X. Y. Zou, P. X. Cai and J. Y. Mo, *Anal. Biochem.*, 2007, **363**, 143–150.
16 L. Wang, Q. Zhang, S. Chen, F. Xu, S. Chen, J. Jia, H. Tan, H. Hou and Y. Song, *Anal. Chem.*, 2014, **86**, 1414–1421.
17 Q. Wang, P. Subramanian, M. S. Li, W. S. Yeap, K. Haenen, Y. Coffinier, R. Boukher-roub and S. Szunerits, *Electrochem. Commun.*, 2013, **34**, 286–290.
18 K. K. Lee, P. Y. Loh, C. H. Sow and W. S. Chin, *Electrochem. Commun.*, 2012, **20**, 128–132.
19 S. A. Zaidi and J. H. Shin, *Talanta*, 2016, **149**, 30–42.
20 V. Mani, R. Devasenathipathy, S. M. Chen, S. F. Wang, P. Devi and Y. Tai, *Electrochim. Acta*, 2015, **176**, 804–810.
21 S. Y. Tee, C. P. Teng and E. Ye, *Mater. Sci. Eng. C*, 2017, **70**, 1018–1030.
22 J. Zhu, J. Jiang, J. Liu, R. Ding, Y. Li, H. Ding, Y. Feng, G. Wei and X. Huang, *RSC Adv.*, 2011, **1**, 1020–1025.
23 C. W. Hsu and G. J. Wang, *Biosens. Bioelectron.*, 2014, **56**, 204–209.
24 X. Niu, M. Lan, H. Zhao and C. Chen, *Anal. Chem.*, 2013, **85**, 3561–3569.
25 C. T. Sousa, D. C. Leitao, M. P. Proenca, J. Ventura, A. M. Pereira and J. P. Araujo, *Appl. Phys. Rev.*, 2014, **1**, 031102.
26 F. Sun, W. Cai, Y. Li, L. C. Jia and F. Lu, *Adv. Mater.*, 2004, **16**, 1116–1121.
27 W. A. El-Said, J. H. Lee, B. K. Oh and J. W. Choi, *Electrochem. Commun.*, 2010, **12**, 1756–1759.
28 Y. Y. Yin, J. W. Zhao, L. R. Qin, Y. Yang and L. Z. He, *Micro Nano Lett.*, 2017, **12**, 128–132.
29 Z. K. Yan, J. W. Zhao, L. R. Qin, F. Mu, P. Wang and X. N. Feng, *Microchim. Acta*, 2013, **180**, 145–150.
30 L. R. Qin, L. Z. He, J. W. Zhao, B. L. Zhao, Y. Y. Yin and Y. Yang, *Sens. Actuators, B*, 2017, **240**, 779–784.
31 F. Sun, L. Li, P. Liu and Y. Lian, *Electroanal*, 2011, **23**, 395–401.
32 L. Zhang, Y. Ni and H. Li, *Microchim. Acta*, 2010, **171**, 103–108.
33 H. F. Tian, M. Z. Jia, M. X. Zhang and J. B. Hu, *Electrochim. Acta*, 2013, **96**, 285–290.
34 J. Yang, M. Cho and Y. Lee, *Sens. Actuators, B*, 2016, **222**, 674–681.
35 M. Zhao, J. Zhao, L. Qin, H. Jia and S. Liu, *J. Electroanal. Chem.*, 2019, **834**, 86–93.
36 L. M. Lu, L. Zhang, F. L. Qu, H. X. Lu, X. B. Zhang, Z. S. Wu, S. Y. Huan, Q. A. Wang, G. L. Shen and R. Q. Yu, *Biosens. Bioelectron.*, 2009, **25**, 218–223.
37 K. Li, G. Fan and L. Yang, *Sens. Actuators, B*, 2014, **199**, 175–182.
38 L. Wang, Q. Zhang, S. Chen, F. Xu, S. Chen, J. Jia, H. Tan, H. Hou and Y. Song, *Anal. Chem.*, 2014, **86**, 1414–1421.
39 H. H. Fan, W. L. Weng, C. Y. Lee and C. N. Liao, *ACS Omega*, 2019, **4**, 12222–12229.
40 Y. Guo, Y. Wang and C. Zhao, *Anal. Methods*, 2013, **5**, 1644–1647.
41 A. Raziq, M. Tariq, R. Hussain, M. H. Mehmood, I. Ullah, J. Khan and M. Muhammad, *J. Serb. Chem. Soc.*, 2018, **83**, 733–744.
42 S. Liu, J. W. Zhao, L. R. Qin, G. Liu, Q. T. Zhang and J. X. Li, *J. Mater. Sci.*, 2020, **55**, 337–346.

